

Rho properties in a hot meson gas

Ralf Rapp¹ and Charles Gale²

1) *Department of Physics and Astronomy, State University of New York, Stony Brook, NY 11794-3800, U.S.A.*

2) *Physics Department, McGill University, Montreal, Quebec H3A 2T8, Canada*

Using effective meson Lagrangians we study the interaction of rho mesons in a hot baryon-free system. Various mesonic resonances in direct s -channel reactions are investigated employing standard self-energy techniques, including new reactions that have up to now not been considered in a self-consistent approach at finite temperature. The importance of subthreshold resonances, which are readily accounted for through off-shell effects within our framework, is emphasized. Special care is taken in reproducing radiative decay widths, as they provide valuable constraints on the evaluation of dilepton spectra. In particular, we compare our results for dilepton production rates to earlier calculations based on an incoherent summation of individual processes.

I. INTRODUCTION

Dilepton measurements in heavy-ion collisions at intermediate [1] and high [2,3] bombarding energies have revealed a strong excess of pairs as compared to proton-induced reactions. It has become clear that the collection of hadronic sources that can successfully account for the measured spectrum in proton-induced reactions fails to reproduce the measured yield in nucleus-nucleus collisions. Even after the inclusion of (free) $\pi^+\pi^-$ annihilation during the interaction phase of the hadronic fireball the enhancement, especially for invariant dilepton masses M_{ll} below the ρ -mass, remained unexplained [4]. Thus many theoretical efforts have concentrated on the role of medium effects in pion and rho meson propagation. It seems fair to say that there currently exists two main schools of thought that have staked a claim onto the theoretical interpretation of the CERN low-mass dilepton measurements. The first one assigns the rho meson mass as an order parameter of the chiral symmetry restoration. The CERN data, in this approach, then signals a dropping of the rho meson mass [5–7]. A second interpretation relies on the fact that in a strongly interacting medium, the rho meson will have its width greatly increased due to modifications of its pion cloud [8–13] as well as to the direct coupling to baryonic resonances [14–17]. Whether these two different scenarios can be reconciled, or whether one of them can be eventually ruled out, is the subject of much current research and debates. In this article we follow the approach that is germane to the second of those theoretical avenues. We will restrict ourselves to a heat bath of pions, kaons and rho mesons, characterized by a finite temperature T . Using the many-body formalism of Ref. [15], we will separately investigate each meson channel and calibrate its individual strength through empirical information on both hadronic and electromagnetic branching ratios, thereby introducing some new channels that have not been considered before in a framework like the one at hand.

The baryon-rich nuclear medium has been shown to strongly affect the vector meson properties, see, *e.g.*, Refs. [15,14,12,17–19]. Then, a self-consistent finite-temperature assessment of the meson contributions is necessary to quantify this assertion. This is particularly true for CERN-SpS energies: in spite of the fact that the phase space is dominated by mesons (with a final pion-to-nucleon ratio of about 5:1), the explanation of the dilepton data in both the dropping mass and the in-medium broadening scenario crucially depends on baryonic contributions. At RHIC energies, however, it is hard to imagine that baryons could play a major role; since dilepton measurements in the PHENIX experiment will be able to address the invariant mass region between $\omega(782)$ and $\phi(1020)$ with excellent resolution, in-medium properties of the rho in mesonic matter should be most relevant there. Various analyses in this direction have already been performed [20–24,15,25]. The moderate collisional broadening for on-shell rho-mesons found in Ref. [22] was mainly attributed to resonant scattering via intermediate $a_1(260)$ and $K_1(1270)$ states. Similar results were obtained in Ref. [15] using finite temperature self-energies which include off-shell effects. This is to be expected, since the $a_1(1260)$ and $K_1(1270)$ are located above the free $\rho\pi$ and ρK thresholds, respectively, which makes the resonant contribution dominant. In order to properly address the low mass region, additional mesons have to be considered. Those larger meson ensembles have in fact been included in calculations where individual rates are summed over [21]. There, the contribution of the ω , for example, appears as a radiative decay channel. In the language used in this work, the ω is a sub-threshold state, *i.e.*, in $\rho\pi \rightarrow \omega(782)$, where, given a typical thermal pion energy of 300–400 MeV, the relevant ρ -mass to form the ω would be substantially off-shell, $M \simeq 400$ MeV.

The objective of this article is twofold: on the one hand, we would like to examine if a consistent off-shell treatment of the most important mesonic resonances has a more severe impact on the dilepton production rates than what has

been estimated so far within different frameworks. At the same time, we can investigate possible interference (or collectivity) effects in the coherent summation of the various self-energy contributions. Since many-body calculations of this nature can be rather convoluted, we will exhibit an explicit channel decomposition of the considered resonances $R = \omega, h_1, a_1, K_1, \pi'$ and f_1 . An upper mass limit of 1.3 GeV enables us to adequately address the phenomenology that concerns us in this work. As the simplest, but by no means negligible, finite temperature effect in the pion cloud of the rho we will furthermore include the Bose-Einstein enhancement in the $\rho \rightarrow \pi\pi$ decay width, which is not new [26,20]. Our paper is organized as follows: the next section introduces the hadronic Lagrangians used in this work, followed by the determination of the parameters in our model in sect. III. We then evaluate the resulting in-medium rho properties (sect. IV) and their impact on dilepton production rates (sect. V). Sect. VI contains a summary and concluding remarks.

II. INTERACTION LAGRANGIANS

Our starting point is the model for the ρ -meson in free space employed previously in Refs. [10,11,15]. Based on the standard $\rho\pi\pi$ interaction vertex (isospin structure suppressed),

$$\mathcal{L}_{\rho\pi\pi} = g_{\rho\pi\pi} \pi p^\mu \pi \rho_\mu, \quad (1)$$

(p^μ : pion momentum) the bare ρ -meson of mass m_ρ^0 is renormalized through the two-pion loop including a once subtracted dispersion relation, giving rise to the vacuum self-energy

$$\begin{aligned} \Sigma_{\rho\pi\pi}^0(M) &= \bar{\Sigma}_{\rho\pi\pi}^0(M) - \bar{\Sigma}_{\rho\pi\pi}^0(0), \\ \bar{\Sigma}_{\rho\pi\pi}^0(M) &= \int \frac{p^2 dp}{(2\pi)^2} v_{\rho\pi\pi}(p)^2 G_{\pi\pi}^0(M, p), \end{aligned} \quad (2)$$

with the vacuum two-pion propagator

$$G_{\pi\pi}^0(M, p) = \frac{1}{\omega_\pi(p)} \frac{1}{M^2 - (2\omega_\pi(p))^2 + i\eta}; \quad \omega_\pi(p) = \sqrt{m_\pi^2 + p^2} \quad (3)$$

and vertex functions

$$v_{\rho\pi\pi}(p) = \sqrt{\frac{2}{3}} g_{\rho\pi\pi} 2p F_{\rho\pi\pi}(p) \quad (4)$$

involving a hadronic (dipole) form factor $F_{\rho\pi\pi}$ [15] (cf. also Eq. (12) below). Resumming the two-pion loops in a Dyson equation gives the free ρ propagator

$$D_\rho^0(M) = [M^2 - (m_\rho^0)^2 - \Sigma_{\rho\pi\pi}^0(M)]^{-1}, \quad (5)$$

which agrees well with the measured p -wave $\pi\pi$ phase shifts and the pion electromagnetic form factor obtained within the vector dominance model (VDM).

To calculate medium corrections to the ρ self-energy in a hot meson gas, we will assume that the interactions are dominated by s -channel resonance formation. At moderate temperatures relevant for the hadronic gas phase, the light pseudoscalar Goldstone bosons $P = \pi, K$ are the most abundant species. We can group the various resonances in ρP collisions in two major categories, namely vector mesons V and axial-vector mesons A . For the latter, a simple interaction Lagrangian, compatible with chiral symmetry and electromagnetic current conservation, is given by

$$\mathcal{L}_{\rho P A} = G_{\rho P A} A_\mu (g^{\mu\nu} q_\alpha p^\alpha - q^\mu p^\nu) \rho_\nu P, \quad (6)$$

although other choices are possible [25]. ρP scattering via intermediate vector mesons V is determined by Wess-Zumino anomaly terms, which are of unnatural parity and involve the four dimensional antisymmetric Levi-Civita tensor $\epsilon^{\mu\nu\sigma\tau}$:

$$\mathcal{L}_{\rho P V} = G_{\rho P V} \epsilon_{\mu\nu\sigma\tau} k^\mu V^\nu q^\sigma \rho^\tau P. \quad (7)$$

In both Lagrangians (6) and (7), p^μ, q^μ and k^μ denote the four-momenta of the pseudoscalar, rho- and (axial-) vector-mesons, respectively. As a third possibility ρP scattering can proceed via a pseudoscalar resonance; here we restrict ourselves to the process $\rho\pi \rightarrow \pi'(1300)$, which can be described by

$$\mathcal{L}_{\rho PP'} = G_{\rho PP'} P' (k \cdot q p_\mu - p \cdot q k_\mu) \rho^\mu P. \quad (8)$$

In addition to that, we will need a ρVA interaction vertex, which is also related to anomaly terms [27]. We choose the following form,

$$\mathcal{L}_{\rho VA} = G_{\rho VA} \epsilon_{\mu\nu\sigma\tau} p^\mu V^\nu \rho^{\sigma\alpha} k_\alpha A^\tau - \frac{\lambda}{2} (k_\beta A^\beta)^2, \quad (9)$$

which again satisfies the appropriate conservation laws. $\rho^{\sigma\alpha} = q^\sigma \rho^\alpha - q^\alpha \rho^\sigma$ is the usual field strength tensor. We have explicitly written here the kinetic energy term of the axial vector field where the constant λ represents a gauge freedom connected with the axial-vector field [28]. In what follows we take $\lambda = 1$; this choice will be further motivated in sect. IV.

An important hint on the importance of resonances in dilepton production is provided by their radiative decay width, which constitutes the $M^2 = 0$ (photon) limit of the timelike dilepton regime. In Table I we have collected mesonic resonances which are accessible via ρ -induced excitations and exhibit substantial decay rates into final states involving either photons or rho-mesons (or both). We expect these to be the relevant contributions to dilepton production. In particular, note that the $f_1(1285)$ has a large radiative decay width of 1.65 MeV for $f_1 \rightarrow \rho\gamma$, which led us to the consideration of the $\rho\rho f_1$ interaction, Eq. (9).

As a first step one has to assign realistic coupling constants in the effective Lagrangians. They are adjusted to the experimental branching ratios of the resonances into, if available, both ρh and γh ($h = \pi, K, \rho$). For reliable estimates of the ρP decay widths it is important to include the finite width of the ρ (in particular for sub-threshold states like the $\omega(782)$ or $f_1(1285)$). This is accomplished by folding the expression for the width at given ρ -mass M with the ρ spectral function $A_\rho^0(M) = -2\text{Im}D_\rho^0(M)$. For the axial-vector meson resonances in ρP scattering the vertex of Eq. (6) leads to

$$\begin{aligned} \Gamma_{A \rightarrow \rho P}(s) &= \frac{G_{\rho PA}^2}{8\pi s} \frac{IF (2I_\rho + 1)}{(2I_A + 1)(2J_A + 1)} \int_{2m_\pi}^{M^{max}} \frac{MdM}{\pi} A_\rho^0(M) q_{cm} \\ &\times \left[\frac{1}{2}(s - M^2 - m_P^2)^2 + M^2 \omega_P(q_{cm})^2 \right] F_{\rho PA}(q_{cm})^2, \end{aligned} \quad (10)$$

and from Eq. (7) one obtains for vector resonances

$$\Gamma_{V \rightarrow \rho P}(s) = \frac{G_{\rho PV}^2}{8\pi} \frac{IF (2I_\rho + 1)}{(2I_V + 1)(2J_V + 1)} \int_{2m_\pi}^{M^{max}} \frac{MdM}{\pi} A_\rho^0(M) 2q_{cm}^3 F_{\rho PV}(q_{cm})^2, \quad (11)$$

with q_{cm} being the three-momentum of the decay products in the resonance rest frame, $\omega_P(q_{cm})^2 = m_P^2 + q_{cm}^2$. IF is an isospin factor, $M^{max} = \sqrt{s} - m_P$, and $F_{\rho PR}$ ($R = A, V$) are hadronic form factors that reflect the finite size of the fields that appear in the effective vertices. We take them to be of dipole form,

$$F_{\rho PR}(q_{cm}) = \left(\frac{2\Lambda_{\rho P}^2 + m_R^2}{2\Lambda_{\rho P}^2 + [\omega_\rho(q_{cm}) + \omega_P(q_{cm})]^2} \right)^2, \quad (12)$$

normalized to 1 at the resonance mass m_R . With the Lagrangian for the pseudoscalar resonance $P' = \pi'(1300)$, Eq. (8), one arrives at

$$\Gamma_{\pi' \rightarrow \rho \pi}(s) = \frac{G_{\rho \pi \pi'}^2}{8\pi} \frac{IF (2I_\rho + 1)}{(2I_{\pi'} + 1)(2J_{\pi'} + 1)} \int_{2m_\pi}^{M^{max}} \frac{MdM}{\pi} A_\rho^0(M) q_{cm}^3 M^2 F_{\rho \pi \pi'}(q_{cm})^2. \quad (13)$$

For the ρVA vertex, which in our case corresponds to the $f_1(1285) \rightarrow \rho\rho$ decay, the spectral functions of both outgoing ρ mesons have to be integrated over. One has

$$\begin{aligned} \Gamma_{f_1 \rightarrow \rho\rho}(s) &= \frac{G_{\rho\rho f_1}^2}{8\pi} \frac{n IF (2I_\rho + 1)}{(2I_{f_1} + 1)(2J_{f_1} + 1)} \int_{2m_\pi}^{M_1^{max}} \frac{M_1 dM_1}{\pi} A_\rho^0(M_1) \int_{2m_\pi}^{M_2^{max}} \frac{M_2 dM_2}{\pi} A_\rho^0(M_2) \\ &\times 2s q_{cm}^3 F_{\rho\rho f_1}(q_{cm})^2, \end{aligned} \quad (14)$$

where the factor $n = 1/2$ ensures the proper symmetrization of the two ρ mesons in the final state. The integration limits are $M_1^{max} = \sqrt{s} - 2m_\pi$, as before, and $M_2^{max} = \sqrt{s} - M_1$.

For each vertex one is left with two unknowns: the coupling constant G and the form factor cutoff Λ_ρ , which should lie in some reasonable region for the hadronic scales at hand, typically $\Lambda_\rho \leq 1 - 2$ GeV. The hadronic decay widths are in fact not very sensitive to Λ_ρ , since the dominant contributions in the M -integrals are centered around the ρ -peak in $A_\rho^0(M)$ (or towards the maximal M if $m_R < m_\rho$), where the three-momenta are rather small. More stringent constraints on Λ_ρ are imposed by the radiative decay widths, since the massless photon can carry away the maximal three-momentum. Invoking the phenomenologically well-established (especially for purely mesonic processes) vector dominance model (VDM), the photon decay widths follow from the hadronic couplings to vector mesons by simply (i) taking the $M^2 \rightarrow 0$ limit, *i.e.*, substituting $A_\rho^0(M) = 2\pi\delta(M^2)$ for real photons, (ii) supplying the VDM coupling constant $(e/g)^2 \simeq 0.052^2$, and, (iii) omitting the $(2I_\rho + 1)$ isospin degeneracy factor for the final state. This yields for both axial-/vector resonances ($R = A, V$)

$$\Gamma_{R \rightarrow \gamma P} = \frac{G_{\rho PR}^2}{8\pi} \left(\frac{e}{g}\right)^2 \frac{IF}{(2I_R + 1)(2J_R + 1)} 2q_{cm}^3 F_{\rho PR}(q_{cm})^2, \quad (15)$$

whereas for the $f_1 \rightarrow \gamma \rho$ decay one still has to integrate over one ρ mass distribution,

$$\Gamma_{f_1 \rightarrow \gamma \rho} = \frac{G_{\rho f_1}^2}{8\pi} \left(\frac{e}{g}\right)^2 \frac{2nIF}{(2I_{f_1} + 1)(2J_{f_1} + 1)} \int_{2m_\pi}^{\sqrt{s}} \frac{M_2 dM_2}{\pi} A_\rho^0(M_2) 2sq_{cm}^3 F_{\rho f_1}(q_{cm})^2. \quad (16)$$

The additional factor of 2 accounts for the two possibilities of attaching the photon to either of the outgoing ρ 's. Within the simple version of VDM employed here, the radiative decay of the $\pi'(1300)$ vanishes.

III. DETERMINATION OF FREE PARAMETERS

Let us now discuss the individual resonances, based on the interaction vertices formulated above, in more detail.

The $\rho\pi a_1(1260)$ coupling constant has been estimated in our framework in Ref. [15] as $G_{\rho\pi a_1} = 13.20$ GeV⁻¹ taking [29] $\Gamma_{a_1 \rightarrow \pi\rho} = 400$ MeV, $m_{a_1} = 1230$ MeV and assuming a cutoff $\Lambda_{\rho\pi a_1} = 2$ GeV. With these parameters the radiative decay width of the a_1 turns out to be 1.23 MeV, somewhat larger than the only available experimental information quoting a value of $\Gamma_{a_1 \rightarrow \pi\gamma} = (0.64 \pm 0.24)$ MeV. This can be substantially improved upon with a reduced cutoff $\Lambda_{\rho\pi a_1} = 1$ GeV, requiring a slightly higher coupling constant $G_{\rho\pi a_1} = 13.27$ GeV⁻¹ to fit the hadronic decay width, but resulting in a photon decay width of $\Gamma_{a_1 \rightarrow \pi\gamma} = 0.66$ MeV, now in good agreement with the experimental value.

The $K_1(1270)$, which was also included in Ref. [15], is the appropriate resonance in ρK scattering. Since there is no radiative decay known, we assume (in analogy to the a_1 cutoff) $\Lambda_{\rho K K_1} = 1$ GeV. Taking $\Gamma_{K_1 \rightarrow K\rho} = 60$ MeV, $m_{K_1} = 1270$ MeV yields $G_{\rho K K_1} = 9.42$ GeV⁻¹, resulting in $\Gamma_{K_1 \rightarrow K\gamma} = 0.32$ MeV, which is qualitatively in line with the naive expectation that in comparison to the a_1 , the heavier strange quark essentially acts as a spectator in the photon decay.

The $h_1(1170)$ is the isospin-0 pendant to the $a_1(1260)$. No quantitative empirical information on its decay properties is available. We therefore make the plausible assumption that the major part of its width originates from the only observed $\rho\pi$ decay channel, *i.e.*, $\Gamma_{h_1 \rightarrow \pi\rho} \simeq 300$ MeV. Using again $\Lambda_{\rho\pi h_1} = 1$ GeV gives $G_{\rho\pi h_1} = 11.37$ GeV⁻¹ and $\Gamma_{h_1 \rightarrow \pi\gamma} = 0.6$ MeV, which seems not unreasonable.

The $\omega(782)$ meson differs from the previously discussed resonances in that it lies significantly below the free $\pi\rho$ threshold. Hadronic models including the effective four-meson $\omega 3\pi$ -vertex usually attribute substantial parts of the hadronic decay width of about 7.5 MeV to $\pi\rho$ states [30]. On the other hand, the radiative decay $\omega \rightarrow \pi\gamma$ should, within VDM, entirely proceed through $\pi\rho$ states. Enforcing the experimentally rather precisely known value of $\Gamma_{\omega \rightarrow \pi\gamma} = 0.72$ MeV, and using again $\Lambda_{\rho\pi\omega} = 1$ GeV, yields the coupling constant $G_{\rho\pi\omega} = 25.8$ GeV⁻¹, entailing $\Gamma_{\omega \rightarrow \pi\rho} = 3.5$ MeV, which is somewhat on the low side of the typical values [30,31]. One could accommodate larger values by choosing softer form factors, but more detailed information should be inferred from the dalitz decay spectrum $\omega \rightarrow \pi^0 \mu^+ \mu^-$, see, *e.g.*, Ref. [32]. Let us point out here that the Dalitz decay $\Gamma_{\omega \rightarrow \pi^0 e^+ e^-}$ is about one order of magnitude larger than the direct dilepton decay width $\Gamma_{\omega \rightarrow e^+ e^-}$ [29].

The $f_1(1285)$ is similar to the $\omega(782)$ in the sense that it is also a sub-threshold state (about 250 MeV below twice the ρ mass), accompanied by a rather small total decay width of ~ 25 MeV; this supports a tempting interpretation as a state with a large $\rho\rho$ component, the decay into it being suppressed by the lack of phase space. We will have more to say on this later. For the time being, if we attribute the entire decay width into 4 pions of about 7.5 MeV

to the $\rho\rho$ channel, the radiative decay is overestimated by at least a factor of 2. Smaller form factor cutoffs are not really efficient in suppressing the radiative decay width, since the latter still involves an integral over one ρ spectral function where dominant contributions arise from masses $M_2 \simeq m_\rho$, where the decay momentum is rather small. A reasonable compromise for our purposes appears to fix the radiative decay width approximately at its experimental value of $\Gamma_{f_1 \rightarrow \rho^0 \gamma} \simeq 1.65$ MeV, which, choosing a form factor cutoff $\Lambda_{\rho\rho f_1} = 0.8$ GeV, results in a hadronic decay width $\Gamma_{f_1 \rightarrow \rho\rho} = 3$ MeV.

The total width of the $\pi(1300)$ is not very well known, quoted as 200-600 MeV by the PDG [29]. Lacking more precise information, we attribute 300 MeV to the $\pi\rho$ channel, which is one of the two observed decay modes. The specific form of our interaction Lagrangian, Eq. (8), together with the VDM assumption, does not allow any radiative decay. The latter has not been observed so far.

The coupling constants and cutoff parameters as well as the resulting branching ratios are summarized in Table II.

IV. IN-MEDIUM ρ PROPAGATOR

Having fixed the parameters of the interaction vertices, we are now set to calculate the in-medium ρ self-energy, Σ_ρ , and corresponding dilepton production rates. The self-energy is related in a standard way to the forward two-body ρ scattering amplitude off the surrounding thermal mesons. Within the imaginary time (Matsubara) formalism one obtains:

$$\Sigma_{\rho h}^{\mu\nu}(q_0, \vec{q}; T) = \int \frac{d^3 p}{(2\pi)^3} \frac{1}{2\omega_h(p)} [f^h(\omega_h(p)) - f^{\rho h}(\omega_h(p) + q_0)] M_{\rho h}^{\mu\nu}(p, q), \quad (17)$$

where the isospin averaged ρ scattering amplitude $M_{\rho h}$ is integrated over the thermal Bose distribution $f^h(\omega_h(p)) = [\exp(\omega_h(p))/T - 1]^{-1}$ of the corresponding hadron species h with $\omega_h(p) = \sqrt{m_h^2 + \vec{p}^2}$. The invariant amplitudes are evaluated in terms of the s -channel resonance contributions from the previous section. Collisions of the ρ with the pseudoscalar mesons $P = \pi, K$ lead to

$$M_{\rho PA}(p, q) = IF G_{\rho PA}^2 F_{\rho PA}(q_{cm})^2 (\varepsilon^\kappa p \cdot q - q^\kappa p \cdot \varepsilon) D_{A, \kappa\lambda}(s) (\varepsilon^{*\lambda} p \cdot q - q^\lambda p \cdot \varepsilon^*) . \quad (18)$$

Then, one obtains for the axial-vector resonances $A = h_1, a_1, K_1$:

$$\begin{aligned} M_{\rho PA}^{\mu\nu}(p, q) &= IF G_{\rho PA}^2 F_{\rho PA}(q_{cm})^2 D_A(s) v_A^{\mu\nu}(p, q) \\ v_A^{\mu\nu}(p, q) &= -g^{\mu\nu}(p \cdot q)^2 + q^\mu q^\nu \frac{(p \cdot q)^2}{s} + (q^\mu p^\nu + q^\nu p^\mu) p \cdot q \left(1 - \frac{q^2}{s}\right) + p^\mu p^\nu q^2 \left(1 - \frac{q^2}{s}\right), \end{aligned} \quad (19)$$

for the vector resonance $V = \omega$:

$$\begin{aligned} M_{\rho PV}(p, q) &= IF G_{\rho PV}^2 F_{\rho PV}(q_{cm})^2 (\varepsilon^{\alpha\kappa\beta\mu} \varepsilon_\mu k_\alpha q_\beta) D_{V, \kappa\lambda}(s) (\varepsilon^{\gamma\lambda\delta\nu} \varepsilon_\nu^* k_\gamma q_\delta), \\ M_{\rho PV}^{\mu\nu}(p, q) &= IF G_{\rho PV}^2 F_{\rho PV}(q_{cm})^2 D_V(s) v_V^{\mu\nu}(p, q), \\ v_V^{\mu\nu}(p, q) &= -g^{\mu\nu}((p \cdot q)^2 - p^2 q^2) - q^\mu q^\nu p^2 + (q^\mu p^\nu + q^\nu p^\mu) p \cdot q - p^\mu p^\nu q^2, \end{aligned} \quad (20)$$

and for the pseudoscalar resonance $\pi'(1300)$:

$$\begin{aligned} M_{\rho PP'}(p, q) &= IF G_{\rho PP'}^2 F_{\rho PP'}(q_{cm})^2 (\varepsilon \cdot p k \cdot q - \varepsilon \cdot k p \cdot q) D_{P'}(s) (\varepsilon^* \cdot p k \cdot q - \varepsilon^* \cdot k p \cdot q), \\ M_{\rho PP'}^{\mu\nu}(p, q) &= IF G_{\rho PP'}^2 F_{\rho PP'}(q_{cm})^2 D_{P'}(s) v_{P'}^{\mu\nu}(p, q), \\ v_{P'}^{\mu\nu}(p, q) &= q^\mu q^\nu (p \cdot q)^2 - (q^\mu p^\nu + q^\nu p^\mu) q^2 p \cdot q + p^\mu p^\nu q^4. \end{aligned} \quad (21)$$

The amplitude tensors $M^{\mu\nu}$ are obtained by removing the ρ meson polarization vectors $\varepsilon_\mu, \varepsilon_\nu^*$ from the invariant matrix elements and contracting the remaining indices. The intermediate (axial-) vector propagators at four-momentum $k \equiv (p + q)$ have been taken as ($R = A, V$)

$$\begin{aligned} D_{R, \kappa\lambda}(k) &= \frac{(-g_{\kappa\lambda} + k_\kappa k_\lambda / s)}{s - m_R^2 + im_R \Gamma_R^{tot}(s)} \\ &\equiv (-g_{\kappa\lambda} + k_\kappa k_\lambda / s) D_R(s). \end{aligned} \quad (22)$$

Using the same form of propagator for the f_1 -meson in the $\rho\rho$ scattering process raises a problem: the corresponding (Born-) amplitude for $\rho\rho \rightarrow f_1 \rightarrow \rho\rho$ vanishes identically, which is, in fact, in line with analyses based on chiral Lagrangians [31,33]. However, the latter then suggests, within VDM, the absence of the direct $f_1 \rightarrow \rho^0\gamma$ decay, which empirically is quite large. Since here we are interested in phenomenological estimates for dilepton production, we decided to circumvent the vanishing $\rho\rho f_1$ coupling by making use of the gauge freedom for massive vector particles provided by the additional $-\frac{\lambda}{2}(k_\beta f_1^\beta)$ -term (Stückelberg term [28]) in the interaction Lagrangian, Eq. (9). With $\lambda = 1$ the f_1 propagator takes the form

$$D_{f_1}^{\kappa\lambda}(s) = -g^{\kappa\lambda}D_{f_1}(s) , \quad (23)$$

which has been used in the actual calculations. We note that when further applying the naive VDM for the two-photon decay of the f_1 , we would obtain a nonzero branching ratio, violating Yang's theorem [34]. This is, of course, an artefact that might be related to our gauge choice (in fact, Brihaye *et al.* [35] pointed out that VDM breaks down at the two-photon level). On the other hand, we have found that the f_1 contributes negligibly to the quantities being calculated in this paper, with the parameters delineated as described above. Therefore, the role of the f_1 , which at first seemed promising because of its large radiative decay width, turned out to be unimportant from a pragmatic point of view, so that we do not attempt further improvements of its interaction vertex.

In the medium, the specification of a thermal rest frame breaks Lorentz invariance. As a consequence, the in-medium ρ self-energy tensor is characterized by two independent scalar functions, each depending separately on energy and three-momentum (in the vacuum one scalar function depending on invariant mass only is sufficient). This is conveniently described in terms of longitudinal and transverse modes of the ρ propagator [20]:

$$D_\rho^{\mu\nu}(q_0, \vec{q}) = \frac{P_L^{\mu\nu}}{M^2 - (m_\rho^0)^2 - \Sigma_\rho^L(q_0, \vec{q})} + \frac{P_T^{\mu\nu}}{M^2 - (m_\rho^0)^2 - \Sigma_\rho^T(q_0, \vec{q})} + \frac{q^\mu q^\nu}{(m_\rho^0)^2 M^2} \quad (24)$$

with the standard projection operators

$$P_L^{\mu\nu} = \frac{q^\mu q^\nu}{M^2} - g^{\mu\nu} - P_T^{\mu\nu} \\ P_T^{\mu\nu} = \begin{cases} 0 & , \mu = 0 \text{ or } \nu = 0 \\ \delta^{ij} - \frac{q^i q^j}{\vec{q}^2} & , \mu, \nu \in \{1, 2, 3\} \end{cases} \quad (25)$$

(the spacelike components of μ and ν are denoted by i and j , respectively). The longitudinal and transverse self-energies are defined by the corresponding decomposition of the polarization tensor:

$$\Sigma_\rho^{\mu\nu}(q_0, \vec{q}) = \Sigma_\rho^L(q_0, \vec{q}) P_L^{\mu\nu} + \Sigma_\rho^T(q_0, \vec{q}) P_T^{\mu\nu} ; \quad (26)$$

they are calculated from Eq. (17) as

$$\Sigma_{\rho PR}^{L,T}(q_0, q) = G_{\rho PR}^2 IF \int \frac{\vec{p}^2 d\vec{p} dx}{(2\pi)^2 2\omega_P(p)} [f^P(\omega_P(p)) - f^{\rho P}(\omega_P(p) + q_0)] F_{\rho PR}(q_{cm})^2 \\ \times D_R(s) v_R^{L,T}(p, q) \quad (27)$$

for $R = A, V, P'$ with $x = \cos\theta$, $\theta = \angle(\vec{p}, \vec{q})$. The projected vertex functions are given by

$$v_A^L(p, q) = (P_L)_{\mu\nu} v_A^{\mu\nu}(p, q) \\ = \frac{q^2}{4s}(s - q^2 - m_\pi^2)^2 + \omega_P(p)^2 q^2(1 - \frac{q^2}{s}) - \vec{p}^2 q^2 x^2(1 - \frac{q^2}{s}) \\ v_A^T(p, q) = \frac{1}{2}(P_T)_{\mu\nu} v_A^{\mu\nu}(p, q) \\ = \frac{1}{2}[\frac{1}{2}(s - q^2 - m_\pi^2)^2 - \vec{p}^2 q^2(1 - x^2)(1 - \frac{q^2}{s})] \\ v_V^L(p, q) = (P_L)_{\mu\nu} v_V^{\mu\nu}(p, q) \\ = q^2 \vec{p}^2(1 - x^2) \\ v_V^T(p, q) = \frac{1}{2}(P_T)_{\mu\nu} v_V^{\mu\nu}(p, q) \\ = \frac{1}{2}[\frac{1}{2}(s - q^2 - m_\pi^2)^2 - 2m_P^2 q^2 - q^2 \vec{p}^2(1 - x^2)] \quad (28)$$

and similar expressions for the pseudoscalar resonance P' . For the $f_1(1285)$ an additional integration over the mass distribution of the ρ from the heat bath has to be performed:

$$\Sigma_{\rho f_1}^{L,T}(q_0, q) = G_{\rho f_1}^2 \int \frac{M_2 dM_2}{\pi} A_\rho(m_2) \int \frac{\vec{p}^2 d|\vec{p}| dx}{(2\pi)^2 2p_0} [f^\rho(p_0) - f^{\rho\rho}(p_0 + q_0)] F_{\rho f_1}(q_{cm})^2 \times D_{f_1}(s) v_{f_1}^{L,T}(p, q), \quad (29)$$

where $M_2^2 = p_0^2 - \vec{p}^2$.

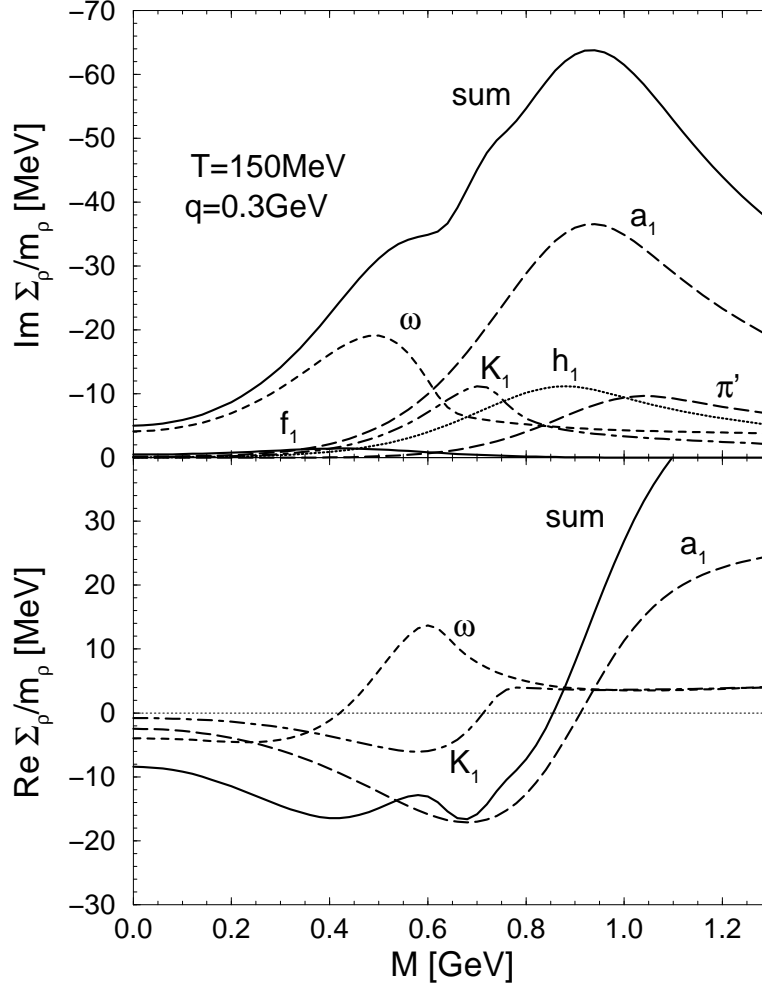


FIG. 1. The real and imaginary parts of the polarization-averaged ρ self-energy (lower and upper panel, respectively). The different channels are labelled explicitly and explained in the text. Note that the $\pi\pi$ channel is absent for the sake of clarity.

In Fig. 1 the real and imaginary parts of the individual spin-averaged self-energy contributions,

$$\Sigma_{\rho h R}(M, q) = \frac{1}{3} [\Sigma_{\rho h R}^L(M, q) + 2\Sigma_{\rho h R}^T(M, q)] , \quad (30)$$

($h = \pi, K, \rho$) are shown at fixed three-momentum modulus $|\vec{q}| = 0.3$ GeV in the lower and upper panel, respectively. Around and above the free mass m_ρ , the strongest absorption is caused by $a_1(1260)$ resonance formation, which is about as large as the sum of all other channels, shared to roughly equal amounts between $K_1(1270)$, $h_1(1170)$ and $\pi'(1300)$. The $K_1(1270)$ curve acquires its maximum at lower M than the pion-resonances due to the higher thermal energies of the kaons (including their rest mass). In the low-mass region $M \leq 0.6$ GeV, the dominant contribution is due to the ω -meson, which, however, barely leaves any trace in the resonance region. It is also seen that the effect of the f_1 is very small. In the real part of the total self-energy we observe appreciable cancellations, until

eventually all contributions turn repulsive (the latter feature would of course be modified when accounting for further higher resonances). Such cancellations are typical for many-body type calculations as performed here. They are the reason that one usually encounters only moderate modifications of the in-medium pole mass. On the other hand, the imaginary parts of Σ_ρ strictly add up, generating significant broadening. We refrain here from plotting the two-pion loop contribution to the ρ self-energy. It will start exceeding the in-medium corrections past $M \simeq 0.450$ GeV (the free ρ width at $M = m_\rho$ amounts to about 150 MeV).

As discussed earlier, the existence of a preferred thermal reference frame will break Lorentz invariance. An advantage of a theoretical approach like the one at hand is that the transverse and longitudinal parts of the rho self-energy can be separately resolved. This is shown on Fig. 2. Even though at the present time one does not have a practical observable that is convincingly sensitive to the polarization, one should keep this difference in mind for future applications [20]. From the figure, we see that at finite three-momentum the polarizations differ the most at low invariant masses and become undistinguishable at high masses.

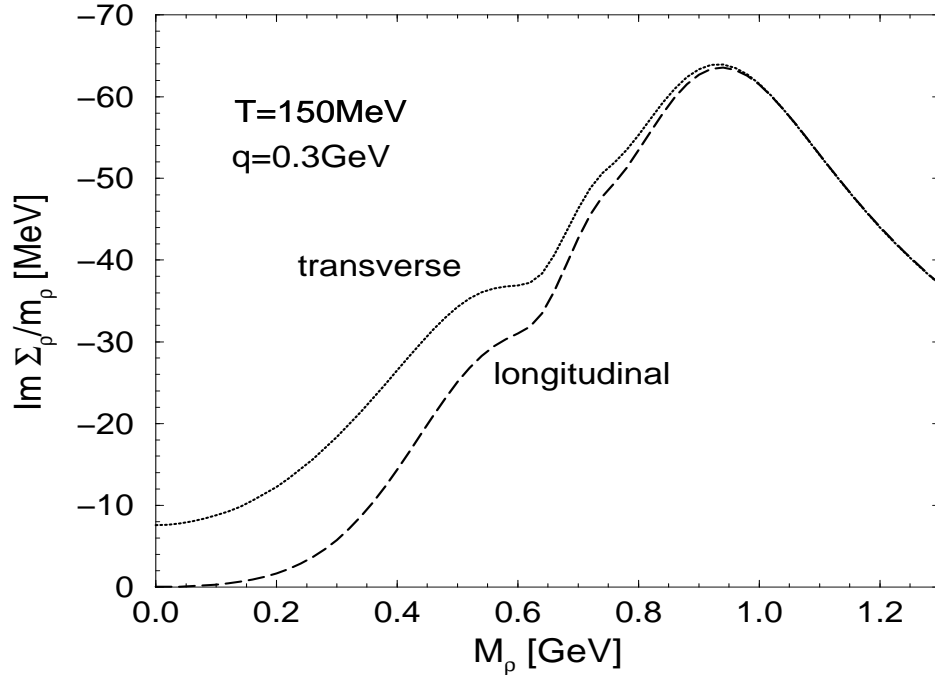


FIG. 2. The longitudinal and transverse polarization contributions to the imaginary part of the self-energy as arising from the sum of meson resonance contributions.

In addition to the direct $\rho - h$ interactions we account for the simplest medium effect in the pion cloud of the ρ by including the Bose enhancement in the two-pion bubble. In the Matsubara formalism this amounts to replacing the two-pion propagator, Eq. (3), by [26]

$$G_{\pi\pi}(M, p; T) = \frac{1}{\omega_\pi(p)} \frac{[1 + 2f^\pi(\omega_\pi(p); T)]}{M^2 - (2\omega_\pi(p))^2 + i\eta} \quad (31)$$

At a temperature of $T = 150$ MeV, this generates an additional broadening of the ρ self-energy starting from the two-pion threshold reaching an appreciable maximum of ~ 20 MeV at $M \simeq 0.6$ GeV (on the scale of Fig. 1, upper panel) and gradually decreasing beyond.

To end this section, we plot in Fig. 3 the full spin-averaged imaginary part of the ρ propagator (spectral function),

$$\text{Im}D_\rho(M, q; T) = \frac{1}{3} [\text{Im}D_\rho^L(M, q; T) + 2\text{Im}D_\rho^T(M, q; T)] \quad (32)$$

in a thermal meson gas of temperatures $T = 120, 150$ and 180 MeV as appropriate for the hadronic phase in ultrarelativistic heavy-ion collisions. More explicitly, one has

$$\text{Im}D_\rho^{L,T}(M, q; T) = \frac{\text{Im}\Sigma_\rho^{L,T}(M, q; T)}{|M^2 - (m_\rho^0)^2 - \Sigma_\rho^{L,T}(M, q; T)|^2} \quad (33)$$

with the longitudinal and transverse self-energy parts

$$\begin{aligned}\Sigma_\rho^L &= \Sigma_{\rho\pi\pi} + \sum_\alpha \Sigma_{\rho\alpha}^L \\ \Sigma_\rho^T &= \Sigma_{\rho\pi\pi} + \sum_\alpha \Sigma_{\rho\alpha}^T,\end{aligned}\tag{34}$$

where the summation is over the mesonic excitation channels $\alpha=\pi\omega$, πh_1 , πa_1 , $\pi\pi'$, KK_1 , $\bar{K}\bar{K}_1$, ρf_1 , as discussed, and $\Sigma_{\rho\pi\pi}$ now contains the Bose-Einstein factors through Eq. (31). We find that the thermal ρ spectral function undergoes a broadening (defined as the full width at half maximum) of about 80 MeV at $T = 150$ MeV (with little three-momentum dependence, see also, *e.g.*, Ref. [15]), which almost doubles to ~ 155 MeV at $T = 180$ MeV. Those values are a factor of 2 larger than the collisional broadening found in Ref. [22] based on on-shell scattering amplitudes. In Ref. [18] the ρ meson self-energy has also been evaluated for on-shell ρ mesons using the $T_{\rho h-qh}$ approximation (*i.e.*, the self-energy being proportional to the ρ - h scattering amplitude and the matter particle density ϱ_h). For a pion gas of density $n_\pi = 1.5 \text{ fm}^{-3}$ a broadening of 400 MeV has been quoted, which, when rescaling to a density of 0.12 fm^{-3} (corresponding to thermal equilibrium at $T = 150$ MeV) gives ~ 30 MeV, again about a factor 2 smaller than our results; this is not surprising as the meson resonances included in ref. [18] were the $a_1(1260)$, $\pi'(1300)$, $a_2(1320)$ and $\omega(1420)$, the latter three contributing rather little at the free ρ mass $M = m_\rho$. On the other hand, the recent kinetic theory treatment performed in Ref. [19] does agree with our findings. However, we would like to stress again that our approach consistently accounts for the empirical radiative decays at the same time, which is crucial for reliable predictions of low-mass dilepton production to be addressed in the next section. The shift of the pole mass, defined by the zero crossing in the real part of the propagator, turns out to be negligible, moving from $M = 773$ MeV in vacuum to $M = 776$ MeV at $T = 150$ MeV.

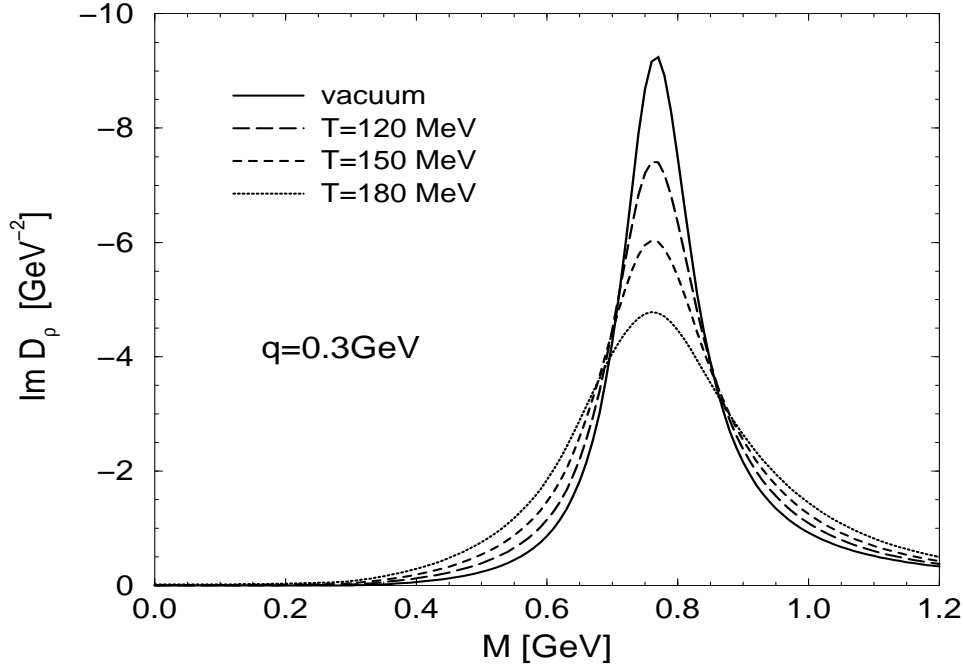


FIG. 3. Imaginary part of the ρ -propagator (spectral function) in the vacuum (dotted curve), and in a thermal gas including the full in-medium self-energies, Eq. (34), for fixed three-momentum $q = 0.3$ GeV at temperatures $T = 120$ MeV (long-dashed curve), $T = 150$ MeV (dashed curve) and $T = 180$ MeV (dotted curve).

V. DILEPTON PRODUCTION

The differential dilepton production rate per unit four-volume and four-momentum in hot matter can be decomposed as [20]

$$\frac{dN_{l^+l^-}}{d^4x d^4q} = L_{\mu\nu}(q) H^{\mu\nu}(q) . \quad (35)$$

For definiteness, we will focus on e^+e^- pairs in the following. Then the electron/positron rest masses can be neglected as compared to their three-momenta, $m_{e^\pm} \ll |\vec{p}_\pm|$, and, to lowest order in the electromagnetic coupling α , the lepton tensor takes the form

$$L_{\mu\nu}(q) = -\frac{\alpha^2}{3\pi^2 M^2} \left(g_{\mu\nu} - \frac{q_\mu q_\nu}{M^2} \right) \quad (36)$$

with the total pair four-momentum $q = p_+ + p_-$. Here, we are interested in dilepton production from ρ decays (or, equivalently, $\pi\pi$ annihilation). Within the VDM, which we have already employed in the evaluation of radiative decay widths in sect. II, the corresponding hadronic tensor is directly related to the imaginary part of the retarded ρ propagator in hot and dense matter:

$$H^{\mu\nu}(q_0, \vec{q}; \mu_B, T) = -f^\rho(q_0; T) \frac{(m_\rho^0)^4}{\pi g_{\rho\pi\pi}^2} \text{Im} D_\rho^{\mu\nu}(q_0, \vec{q}; \mu_B, T) . \quad (37)$$

Using the decomposition Eq. (24), the dilepton rate can then be written as

$$\frac{dN}{d^4x d^4q} = -\frac{\alpha^2 (m_\rho^0)^4}{\pi^3 g_{\rho\pi\pi}^2} \frac{f^\rho(q_0; T)}{M^2} \frac{1}{3} [\text{Im} D_\rho^L(q_0, q; T) + 2 \text{Im} D_\rho^T(q_0, q; T)] \quad (38)$$

with the longitudinal and transverse spectral functions given by Eq. (33).

In Fig. 4 we display the individual medium effects in the three-momentum integrated rates

$$\frac{dN}{d^4x dM^2}(M; T) = \int \frac{d^3q}{2q_0} \frac{dN}{d^4x d^4q}(q_0, \vec{q}) . \quad (39)$$

for electron-positron production at a fixed temperature of $T=150$ MeV. The two mechanisms that dominate the net

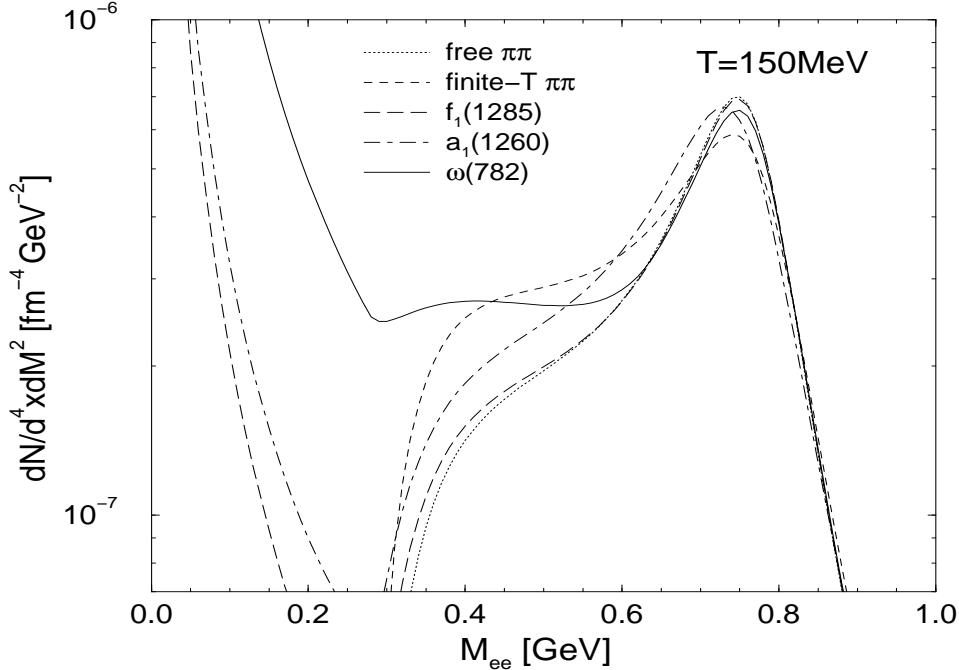


FIG. 4. Three-momentum integrated dilepton production rates at temperature of $T = 150$ MeV including various individual medium effects in the ρ propagator (see Eqs. (38), (33), (34)); dotted curve: free $\pi\pi$ annihilation (*i.e.*, using $\Sigma_\rho^{L,T} = \Sigma_{\rho\pi\pi}^0$); short-dashed curve: $\pi\pi$ annihilation including finite temperature effects through Bose enhancement factors, Eq. (31) (using $\Sigma_\rho^{L,T} = \Sigma_{\rho\pi\pi}$); long-dashed curve: free $\pi\pi$ including $\rho\rho \rightarrow f_1$ resonance formation (using $\Sigma_\rho^{L,T} = \Sigma_{\rho\pi\pi}^0 + \Sigma_{\rho\rho f_1}^{L,T}$); dashed-dotted curve: free $\pi\pi$ including $\rho\pi \rightarrow a_1$ resonance formation (using $\Sigma_\rho^{L,T} = \Sigma_{\rho\pi\pi}^0 + \Sigma_{\rho\pi a_1}^{L,T}$); solid curve: free $\pi\pi$ including $\rho\pi \rightarrow \omega$ resonance formation (using $\Sigma_\rho^{L,T} = \Sigma_{\rho\pi\pi}^0 + \Sigma_{\rho\pi\omega}^{L,T}$).

low-mass dilepton rate are associated with $\rho\pi \rightarrow \omega$ formation as well as the Bose-Einstein (BE) enhancement of the $\rho \rightarrow \pi\pi$ decay width. *E.g.*, at $M=0.4$ GeV, both the ω (solid line) and the finite- T (BE) corrections in the pion cloud enhance the free $\pi\pi$ annihilation rate by (80-90)% each. Much smaller effects are due to the $a_1(1260)$ (30% enhancement, dashed-dotted line) as well as the K_1 and h_1 (20% and 15% enhancement, respectively, not shown in Fig. 4), the f_1 being practically negligible.

In Fig. 5 we compare the total rate calculated from an incoherent sum of meson reactions and decays [21] (dashed-dotted line) with our full result (solid line). Focusing again at $M = 0.4$ GeV, the latter is increased over the free $\pi\pi$ result (=GL, dotted line) by a factor of 3.5, compared to ~ 2 in the Gale-Lichard calculation. The major difference arises from the inclusion of the BE-enhancement (and, to a lesser extent, the a_1/h_1 resonances) in the present treatment. Also shown in Fig. 5 are the results based on the finite temperature part of the calculation by Rapp, Chanfray and Wambach (=RCW, short-dashed curve) [15], which included a_1 , K_1 resonances and the Bose-Einstein enhancement in $\Sigma_{\rho\pi\pi}$ (note, however, that the hadronic form factors used in Ref. [15] were substantially harder, with cutoffs $\Lambda_{\pi\rho a_1} = \Lambda_{K\rho K_1} = 2$ GeV; this entails an overestimation of the *radiative* $a_1 \rightarrow \gamma\pi$ decay width by a factor of 2, as elaborated in sect. III). Consequently, in the vicinity of the free ρ mass, where the major broadening effect is due to a_1 formation and BE-enhancement, the RCW results differ very little from the present ones. Below, ω formation in $\rho\pi$ scattering is responsible for a substantial increase of the emission rate (full curve compared to short-dashed curve).

Another point is finally noteworthy of attention: if one looks at the total spectrum in the vicinity of the *rho*-peak, one sees that the net signal in our many-body spectral function approach is reduced by about 40% as compared to free $\pi\pi$ annihilation. As discussed in the previous section, the shift of the real part is very small (a few MeV; the *apparent* larger shift in the dilepton spectrum is caused by the overall Bose factor in the rate expression, Eq. (38), which strongly increases towards smaller invariant masses), but the broadening of ~ 80 MeV is appreciable on the scale of the free ρ width of ~ 150 MeV. The resulting peak smearing is a distinct feature of our many-body formalism, *i.e.*, the resummation encoded in the denominator in Eq. (33), which is neither present in the rate calculations of Ref. [21] nor in low-density expansions as performed, *e.g.*, in Ref. [24]. This feature will be tested against experiment soon, as a result of improving the mass resolution in the CERES experiment at CERN-SpS energies, as well as at RHIC energies in the PHENIX detector, where the design value for $\Delta M/M$ is at the 1% level.

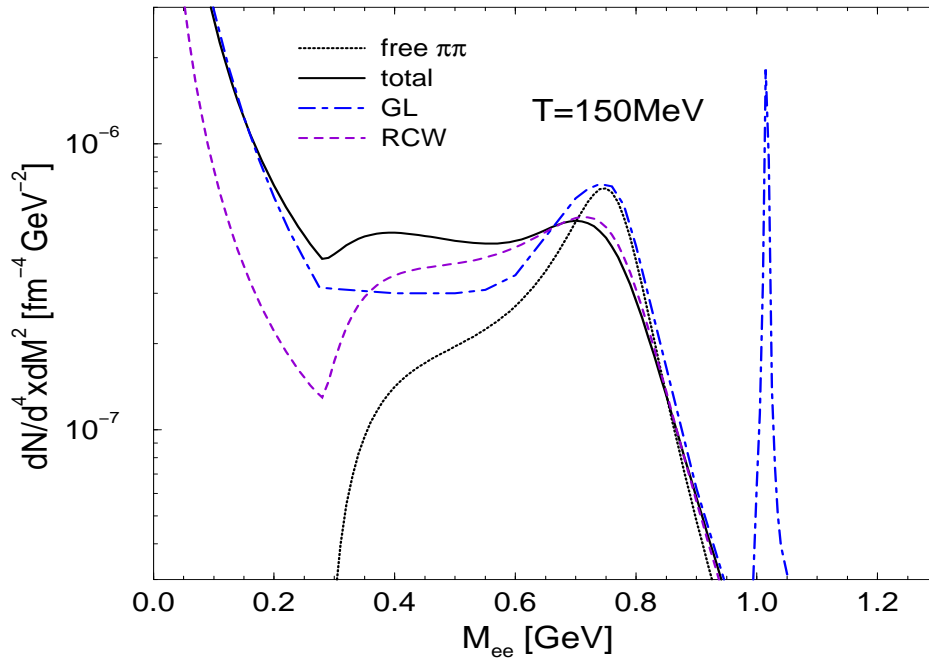


FIG. 5. Comparison of our total, three-momentum integrated thermal dilepton production rate (solid curve) with that obtained from a sum of meson decays and reactions according to Ref. [21] (dashed-dotted curve). The dotted curve represents the rate obtained from free $\pi\pi$ annihilation, whereas the dashed curve corresponds to the finite temperature part of the many-body calculation of Ref. [15]. All curves are for a fixed temperature $T = 150$ MeV.

VI. SUMMARY AND CONCLUSIONS

Based on a finite temperature (Matsubara) formalism we have highlighted different interaction channels that could lead to modifications of the rho properties in a thermal gas of mesons with zero chemical potentials. Using phenomenological interaction vertices compatible with gauge invariance and chiral symmetry, and including hadronic form factors to simulate finite size effects, the free parameters could be tuned to reproduce the empirical hadronic *and* radiative decay branchings rather well. The resulting in-medium ρ self-energy induces a moderate broadening of the ρ spectral function, somewhat higher than what has been found before in Refs. [22,15,18], but consistent with a recent kinetic theory analysis [19]. On the other hand, cancellations in the real part inhibited significant changes of the in-medium ρ pole-mass. Corresponding dilepton spectra exhibit a 40% depletion of the ρ -peak together with an appreciable enhancement of a factor of ~ 3.5 below, largely driven by sub-threshold $\pi\rho \rightarrow \omega$ formation and a Bose enhancement in the $\rho \rightarrow \pi\pi$ width. Our results have now to be combined with those obtained with the baryons present, and a time-evolution approach will be coupled with our rates to produce yields that can be compared with experiment.

Finally, for the sake of comparison, we have overlayed our results with the those obtained from an (incoherent) sum of meson reactions and decays [21]. Some differences emerge: the earlier calculations in Ref. [21] do not include the contribution that can be associated with the radiative decay of the $a_1(1260)$ and $h_1(1170)$; also, the VDM form factor used there was temperature-independent. The methods employed in this work are tantamount to the generation of a temperature-dependent form factor. Besides that, it seems that the self-consistent many-body treatment does not induce large deviations as compared with the results of (incoherent) rate calculations as far as the low-mass enhancement is concerned. There are, of course, significant differences around the free ρ mass, in that the many-body calculations lead to a reduction of the ρ -peak. In fact, these features can be understood in a rather transparent way as follows. Schematically, the ρ spectral function (which directly governs the dilepton rate) can be written in terms of the self-energy as

$$\text{Im}D_\rho = \frac{\text{Im}\Sigma_\rho}{|M^2 - m_\rho^2|^2 + |\text{Im}\Sigma_\rho|^2}, \quad (40)$$

where we have absorbed the real part of the self-energy in the (physical) ρ mass m_ρ . In the low-mass region, where $m_\rho \gg M$ and $m_\rho \gg |\text{Im}\Sigma_\rho|$, the denominator is dominated by m_ρ so that

$$\text{Im}D_\rho(M \ll m_\rho) \propto \frac{\text{Im}\Sigma_\rho}{m_\rho^4}. \quad (41)$$

Since $\text{Im}\Sigma_\rho$ corresponds to a summation of scattering amplitudes times (pion-) density, one immediately recognizes the close resemblance to kinetic theory or low-density expansion approaches. On the other hand, in the vicinity of the ρ -peak, where $M \simeq m_\rho$, the denominator in Eq. (40) is dominated by $\text{Im}\Sigma_\rho$ so that

$$\text{Im}D_\rho(M \simeq m_\rho) \propto \frac{1}{\text{Im}\Sigma_\rho}, \quad (42)$$

demonstrating that the consequence of an increase in density is a suppression of the maximum, which cannot be straightforwardly casted in a low-density expansion.

Overall, however, the finite temperature effects found here are still to be regarded as rather moderate. On the contrary, the nuclear environment has a much stronger impact on the in-medium rho-modifications at comparable densities [15,12,17–19]: *e.g.*, at a temperature $T = 160$ MeV, where the thermal pion density, $n_\pi = 0.16 \text{ fm}^{-3}$, equals normal nuclear density, the ρ spectral function broadens by about $\Gamma_\rho^{\text{med}}(T = 160\text{MeV}) \simeq 100 \text{ MeV}$, which is considerably less than in nuclear matter ($\Gamma_\rho^{\text{med}}(\rho_N = \rho_0) \geq 300 \text{ MeV}$, as extracted, *e.g.*, from Refs. [16,36]). From a theoretical point of view this state of affairs may appear puzzling, since towards the chiral restoration transition, which is to be expected around the temperatures considered here, a substantial reshaping of the vector and axial-vector spectral distribution must occur: for $T \geq T_c^x$, they have to become degenerate as an unavoidable consequence of the (approximate) chiral symmetry in the strong interactions. The reason for this discrepancy may be related to the fact that in the heat bath the ρ modifications as calculated in the present article are still hindered by the Goldstone nature of the pions. This observation does not apply to ρ -interactions with nucleons in the finite density case. A complete understanding still requires further elucidation.

Resuming one of the motivations of our analysis, we believe that the understanding of complex strongly interacting systems that live in regions of density and temperature far removed from equilibrium resides not only in confronting theoretical calculations with experimental data, but also in comparing the theories among themselves.

ACKNOWLEDGMENTS

We are grateful for productive conversations with M. Wachs, J. Wambach and I. Zahed. One of us (R. R.) acknowledges support from the Alexander-von-Humboldt foundation as a Feodor-Lynen fellow and thanks C. Gale for the hospitality during his visit to Montreal. C.G. is grateful to the Nuclear Theory Group of the State University of New York at Stony Brook for its hospitality during part of a sabbatical leave, when this work was initiated. This work is supported in part by the U.S. Department of Energy under Grant No. DE-FG02-88ER40388, the Natural Sciences and Engineering Research Council of Canada and the Fonds FCAR of the Quebec Government.

-
- [1] R.J. Porter et al., Phys. Rev. Lett. **79**, 1229 (1997).
 - [2] G. Agakichiev *et al.*, CERES collaboration, Phys. Rev. Lett. **75**, 1272 (1995);
P. Wurm for the CERES collaboration, Nucl. Phys. **A590**, 103c (1995).
 - [3] N. Masera for the HELIOS-3 collaboration, Nucl. Phys. **A590**, 93c (1995).
 - [4] See, for example, A. Drees, Nucl. Phys. **A630**, 449c (1998), and references therein.
 - [5] G.E. Brown and M. Rho, Phys. Rev. Lett. **66**, 2720 (1991).
 - [6] W. Cassing, W. Ehehalt and C.M. Ko, Phys. Lett. **B363**, 35 (1995).
 - [7] G.Q. Li, C.M. Ko and G.E. Brown, Phys. Rev. Lett. **75**, 4007 (1995); Nucl. Phys. **A606**, 568 (1996).
 - [8] M. Asakawa, C. M. Ko, P. Lévai and X. J. Qiu, Phys. Rev. **C46**, R1159 (1992).
 - [9] M. Herrmann, B. Friman and W. Nörenberg, Nucl. Phys. **A560**, 411 (1993).
 - [10] G. Chanfray and P. Schuck, Nucl. Phys. **A555**, 329 (1993).
 - [11] G. Chanfray, R. Rapp and J. Wambach, Phys. Rev. Lett. **76**, 368 (1996).
 - [12] F. Klingl, N. Kaiser and W. Weise, Nucl. Phys. **A624**, 527 (1997).
 - [13] M. Urban, M. Buballa, R. Rapp and J. Wambach, Nucl. Phys. **A641**, 433 (1998).
 - [14] B. Friman and H.J. Pirner, Nucl. Phys. **A617**, 496 (1997).
 - [15] R. Rapp, G. Chanfray and J. Wambach, Nucl. Phys. **A617**, 472 (1997).
 - [16] R. Rapp, M. Urban, M. Buballa and J. Wambach, Phys. Lett. **B417**, 1 (1998).
 - [17] W. Peters, M. Post, H. Lenske, S. Leupold and U. Mosel, Nucl. Phys. **A632**, 109 (1998).
 - [18] V.L. Eletsky, B.L. Ioffe, and J.I. Kapusta, Eur. Phys. J. **A3**, 381 (1998);
V. L. Eletsky and J. I. Kapusta, nucl-th/9810052.
 - [19] S. Gao, C. Gale, C. Ernst, H. Stöcker and W. Greiner, nucl-th/9812059.
 - [20] C. Gale and J. Kapusta, Nucl. Phys. **B357**, 65 (1991).
 - [21] C. Gale and P. Lichard, Phys. Rev. D **49**, 3338 (1994).
 - [22] K. Haglin, Nucl. Phys. **A584**, 719 (1995); Phys. Rev. **C53**, R2606 (1996).
 - [23] C. Song, V. Koch, S.H. Lee and C.M. Ko Phys. Lett. **B366**, 379 (1996);
C. Song and V. Koch, Phys. Rev. **C54**, 3218 (1996).
 - [24] J.V. Steele, H. Yamagishi and I. Zahed, Phys. Lett. **B384**, 255 (1996).
 - [25] S. Gao and C. Gale, Phys. Rev. C **57**, 254 (1998).
 - [26] T. Hatsuda and T. Kunihiro, Prog. Theo. Phys. **91**, 284 (1987).
 - [27] N. Kaiser and U.-G. Meissner, Nucl. Phys. **A519**, 671 (1990).
 - [28] C. Itzykson and J.B. Zuber, *Quantum Field Theory* (McGraw Hill, New York, 1980).
 - [29] Particle Data Group, R.M. Barnett *et al.*, Phys. Rev. **D54**, 1 (1996).
 - [30] M. Gell-Mann, D. Sharp, and W. G. Wagner, Phys. Rev. Lett. **8**, 61 (1962).
 - [31] Bing An Li, Phys. Rev. D **52**, 5165 (1995).
 - [32] F. Klingl, N. Kaiser and W. Weise, Zeit. Phys. **A356**, 193 (1996).
 - [33] H. Gomm, O. Kaymakcalan, and J. Schechter, Phys. Rev. D **30**, 594 (1984).
 - [34] C. N. Yang, Phys. Rev. **77**, 242 (1950).
 - [35] Y. Brihaye, N.K. Pak and P. Rossi, Nucl. Phys. **B254** 71, (1985).
 - [36] R. Rapp, Proceedings of the 33rd Recontres de Moriond on “QCD and High Energy Hadronic Interactions”, Les Arcs (France), March 21-28, 1998, published in Edition Frontiers, ed. J. Tran Thanh Van, and nucl-th/9804065.

TABLES

R	$I^G J^P$	Γ_{tot} [MeV]	ρh Decay	$\Gamma_{\rho h}^0$ [MeV]	$\Gamma_{\gamma h}^0$ [MeV]
$\omega(782)$	$0^- 1^-$	8.43	$\rho\pi$	~ 5	0.72
$h_1(1170)$	$0^- 1^+$	~ 360	$\rho\pi$	seen	?
$a_1(1260)$	$1^- 1^+$	~ 400	$\rho\pi$	dominant	0.64
$K_1(1270)$	$\frac{1}{2} 1^+$	~ 90	ρK	~ 60	?
$f_1(1285)$	$0^+ 1^+$	25	$\rho\rho$	≤ 8	1.65
$\pi'(1300)$	$1^- 0^-$	~ 400	$\rho\pi$	seen	?

TABLE I. Mesonic Resonances R with masses $m_R \leq 1300$ MeV and substantial branching ratios into final states involving direct ρ 's (hadronic) or ρ -like photons (radiative).

R	$IF(\rho h R)$	$G_{\rho h R}$ [GeV^{-1}]	$\Lambda_{\rho h R}$ [MeV]	$\Gamma_{\rho h}^0$ [MeV]	$\Gamma_{\gamma h}^0$ [MeV]
$\omega(782)$	1	25.8	1000	3.5	0.72
$h_1(1170)$	1	11.37	1000	300	0.60
$a_1(1260)$	2	13.27	1000	400	0.66
$K_1(1270)$	2	9.42	1000	60	0.32
$f_1(1285)$	1	35.7	800	3	1.67
$\pi'(1300)$	2	9.67	1000	300	0

TABLE II. Results of our fit to the decay properties of ρ - h induced mesonic resonances R with masses $m_R \leq 1300$ MeV (the $f_1(1285)$ and $\pi'(1300)$ coupling constants are in units of GeV^{-2}).